ELSEVIER

Polymer 43 (2002) 467–476

polymer

www.elsevier.com/locate/polymer

Structure and dynamics of thin polymer films: a case study with the bond-fluctuation model ☆

C. Mischler[a], J. Baschnagel[b,*], S. Dasgupta[c], K. Binder[a]

[a]*Institut für Physik, Johannes-Gutenberg Universität, D-55099 Mainz, Germany*
[b]*Institut Charles Sadron, 6 rue Boussingault, F-67083 Strasbourg Cedex, France*
[c]*Department of Physics, University of Calcutta, 92 A.P.C. Road, Calcutta 700009, India*

Abstract

This paper reports Monte Carlo simulation results of a polymer melt of short, non-entangled chains which are embedded between two impenetrable walls. The melt is simulated by the bond-fluctuation lattice model under athermal conditions, i.e. only excluded volume interactions between the monomers and between the monomers and the walls are taken into account. In the simulations, the wall separation is varied from about one to about 15 times the bulk radius of gyration R_g. The confinement influences both static and dynamic properties of the films: Chains close to the walls preferentially orient parallel to it. This parallel orientation decays with increasing distances from the wall and vanishes for distances larger than about $2R_g$. Strong confinement effects are therefore observed for film thicknesses $D \lesssim 4R_g$. The preferential alignment of the chains with respect to the walls suppresses reorientations in perpendicular direction, whereas parallel reorientations take place in an environment of high monomer density. Therefore, they have a relaxation time larger than that of the bulk. On the other hand, the influence of confinement on the translation motion of the chains parallel to the walls is very weak. It almost coincides with the bulk behavior even if $D \approx 1.5R_g$. Despite these differences between translational and reorientational dynamics, their behavior can be well reproduced by a variant of Rouse theory which only assumes orthogonality of the Rouse modes and determines the necessary input from the simulation.

PACS: 68.15. + e; 61.20.Ja; 61.25.Hq

Keywords: Polymer films; Bond-fluctuation model; Monte Carlo simulation

1. Introduction

Interfacial properties of polymeric films represent an interesting field of applied and fundamental research [1–5]. Even if one ignores complications occurring at the interface between polymer and substrate in real materials, such as corrugation on atomistic scale, roughness on mesoscopic scale or adsorbed impurities, and models the underlying substrate as a completely smooth wall, the properties of the chains close to the wall substantially deviate from the established bulk behavior [2–4]. The deviations depend on the polymer–substrate interaction and external control parameters, such as film thickness, pressure or temperature.

If the interaction between the wall and all monomers of the polymers is attractive, the chains adsorb below the adsorption temperature T_a [5,6]. Above T_a, the reduction of orientational freedom leads to a depletion of chains near the wall, whereas the gain in interaction energy outweighs this loss in entropy below T_a. The adsorbed chains have strongly flattened, almost two-dimensional configurations contrary to the random coil structure in the bulk [7–13]. The thermodynamic properties of the adsorbed layer has been extensively studied both numerically [6,12–15] and analytically [2,16–20].

On the other hand, if there is no preferential attraction between the monomers and the wall, but the wall merely represents an impenetrable obstacle, the situation resembles the aforementioned attractive case for $T > T_a$. In dilute solution, the loss of orientational entropy makes the monomer and chain concentrations vanish at the wall. As the bulk density increases, the packing constraints of all chains gradually compensate the loss in entropy. At melt-like densities, the monomer profile develops pronounced oscillations, which are damped out

☆ This paper was originally submitted to *Computational and Theoretical Polymer Science* and received on 22 November 2000; received in revised form on 23 February 2001; accepted on 25 February 2001. Following the incorporation of *Computational and Theoretical Polymer Science* into *Polymer*, this paper was consequently accepted for publication in *Polymer*.

* Corresponding author. Tel.: +33-8841-4059; fax: +33-8841-4099.
E-mail address: baschnag@ics.u-strasbg.fr (J. Baschnagel).

0032-3861/02/$ - see front matter
PII: S0032-3861(01)00423-2

after a few interparticle distances and can be interpreted similarly to those of the pair-distribution function in bulk fluids. These oscillations are observed in simulations [4,7,10,11,21,22] and can also be rationalized analytically [23–30].

Whereas these static features of polymer films are well established, a similar level of understanding for the dynamic properties has not yet been reached. However, one would expect the influence of confinement on the polymer structure to carry over to the dynamic properties of the melt. In fact, computer simulations suggest that the mobility of chains close to a hard wall increases in parallel, but decreases in perpendicular direction, relative to the isotropic bulk value [4,7,10,11,31,32]. This anisotropy is usually rationalized as a consequence of those chain portions which are in immediate contact with the wall. Their mobility should be facilitated in parallel direction due to both the preferentially parallel alignment of the chains and the smooth walls. In agreement with this interpretation, one finds that the motion of the polymers approaches the isotropic bulk behavior on the same length scale as the chain density profile (on the scale of the bulk radius of gyration R_g) [4,7,10,11,31].

These findings are not limited to polymer films confined between two solid walls. Recent Monte Carlo simulations for a coarse-grained lattice model, suitably adapted to efficiently simulate polyethylene [33–35], illustrate the same dynamic anisotropy between parallel and perpendicular motions also for free-standing film (two vacuum-polymer surfaces) [36], nanofibers [37] and supported films (free surface on one side and solid (partially attractive) substrate on the other side) [38].

From a theoretical point of view, it would also be interesting to test to what extent widely studied models, such as the Rouse model [39], can be applied to the polymer dynamics in confined geometry. In the bulk, this model is often suggested as a viable approximation to the dynamics of short chains [39–41] and furthermore underlies the reptation theory for the dynamics of long chains [39]. So, a more detailed test of its applicability in confined geometry might be beneficial.

The present paper describes results of such an application of the Rouse model to Monte Carlo simulations of a simple lattice model for a non-entangled polymer melt which is embedded between two impenetrable walls. Special attention is paid to the influence of film thickness on the dynamics (and statics) of the melt. The thickness D is varied from $D \approx 1.5R_g$ to $D \approx 1.5R_g$, thus encompassing the regime of strong to weak spatial confinement. The paper is organized as follows: Section 2 introduces the model of the simulation; the following two sections summarize the results. Section 3 discusses some static properties, whereas Section 4 is devoted to the dynamics of the films. Section 5 contains our conclusions.

2. Simulation model

The model of the simulation has been described in detail in Refs. [22,42]. Here, we only give a brief outline of its properties. The present approach uses a lattice model: the bond-fluctuation model [43–46]. A monomer of this model does not correspond to a single lattice site, but to a whole unit cell of a simple cubic lattice. This enlarged size of a monomer allows the bond vectors to fluctuate both in length and direction. The fluctuation of the bond length b is limited to the interval $2 \le b \le 10^{1/2}$ to automatically guarantee local self-avoidance of the monomers and uncrossability of the bond vectors during the simulation. Since only excluded volume interactions are taken into account, the simulated situation corresponds to the high temperature, fluid regime of the polymer films (formally $T = \infty$).

A chain of the model consists of $N = 10$ monomers. This chain length is shorter than the entanglement degree of polymerization ($N_e \approx 37$ [47,48]). Therefore, the Rouse model should provide a reasonable description of the polymer dynamics in the melt [39]. To set up a melt K chains are placed in a rectangular simulation box of size $L \times L \times D$. The number of chains is adjusted so that the volume fraction of occupied lattice sites is $\phi = 8NK/DL^2 = 0.5\bar{3}$. At volume fractions $\phi \ge 0.5$, the bond-fluctuation model exhibits typical features of dense melts [49,50]. The dimension of the simulation box parallel to the walls is chosen to be $L = 60$ (in units of the lattice constant). The choice guarantees that half of the box length is larger than the maximum end-to-end distance of a chain. This prevents finite-size effects [22]. In the parallel directions, periodic boundary conditions are applied, whereas the simulation box is confined by two completely smooth, hard walls, situated at $z = 1$ and $z = D$, in the perpendicular direction. Effectively, this simulates an infinitely long polymer film embedded between two equivalent, inert substrates. The film thicknesses studied extend from $D = 6$ ($\approx 1.5R_g$) to $D = 60$ ($\approx 15R_g$). Depending on the system under consideration, the total number of simulated monomers ranges between 43,200 and 86,400 to obtain sufficient statistics.

The simulation employs two kinds of dynamic algorithms: a local random hopping and the non-local slithering-snake algorithm [51,52]. The slithering-snake algorithm attempts to attach a new, randomly chosen bond vector to one end of a chain (also randomly chosen). If the attempt does not violate the excluded volume condition (no lattice site may be occupied doubly), it is accepted and the last bond vector of the opposite chain end is removed. This algorithm is non-local because the whole chain is shifted over the distance of one bond during the move. Of course, such a 'cut-and-paste' algorithm does not mimic the real polymer dynamics. It is an artificial procedure which, however, allows one to rapidly equilibrate the melt [53]. Therefore, we used this method to generate equilibrated

start configurations for the local random hopping algorithm.[1] Contrary to the slithering-snake moves, local random hopping is physically more realistic. In this scheme, a monomer and a lattice direction are first chosen at random. Then, a displacement of the monomer in this direction is proposed, and it is checked whether the target sites are empty (excluded volume interaction) and whether the new bonds belong to the allowed set of bond vectors (maintenance of chain connectivity). If these conditions are satisfied, the move is accepted. These local moves can be thought of as resulting from a local random force exerted on a monomer by its environment. They lead to Rouse-like dynamics which is typical of short polymers in dense melts [39–41]. Therefore, we used the local random hopping algorithm to investigate the dynamic properties of our system.

3. Static properties of the polymer films

Theoretical studies [2,5,17,23–30], computer simulations [4,6,7,9,21,32,54], and some recent experiments [55] (see however Ref. [56] for different experimental observations) suggest that the structure of a melt close to an impenetrable interface is different from that of the bulk. Since the interface restricts the number of accessible configurations, the chains prefer to stay away from it. This repulsive force has to compete with the density of the system: in a dense melt, it is not possible to deplete the vicinity of the interface without concentrating the inner portion of the film. This increase in density yields a force, which tends to push the polymers towards the interface.

The superposition of both forces leads to the following situation: there are very few chains whose center of mass is situated at the interface. Those chains are oriented parallel to wall and flattened. With increasing distance from the interface, the parallel alignment gradually randomizes and the chains adopt their bulk-like (ellipsoidal [57–62]) shape. This crossover from the wall to the bulk behavior extends over a zone of size of about $2R_g$ next to the interface. Chains in this zone contribute to enhanced monomer and end-monomer densities at the interface, which gives rise to characteristic density oscillations around the bulk density: a high density at the interface imposes a small density in the adjacent layer due to excluded volume interactions, which in turn allows a higher density in the subsequent layer and so on until the bulk value is reached. These and other density profiles probing the length scale of a monomer and of a chain have been studied in detail for the present model [42,63] and the results were reviewed in Ref. [54] and more recently in Refs. [21,22]. Therefore, we just want to discuss one example in the following and then pass on to static correlations of the Rouse modes, which represent an important input for the subsequent analysis of the dynamic properties of the films.

3.1. Profile of the end-to-end distance

Fig. 1 shows the profile of the end-to-end distance $R^2_{ee}(z_{cm})$, measured parallel and perpendicular to the walls. Here, 'parallel' means an average of the x- and y-components of $R^2_{ee}(z_{cm})$, over all chains whose center of mass is situated at a distance z_{cm} from the (left) wall. 'Perpendicular' refers to an analogous average of the z-component of $R^2_{ee}(z_{cm})$.

In order to interpret Fig. 1, one has to take account of the fact that the instantaneous structure of a polymer resembles a 'soap-shaped' ellipsoid [57–62]. Far away from the wall, the film behaves as the unconstrained bulk. The ellipsoid can orient freely and the polymer appears spherical on average. The bulk-like inner part extends from the middle of film to about $z_{cm} \approx 2R_g = 7.36$, where the interfacial region starts. Since the melt is confined between two walls, such an inner part can only be observed if $D \gtrsim 18$ ($\approx 5R_g$). For smaller thicknesses, ($D \lesssim 12 \approx 3R_g$) the film just consists of interfacial region because the perturbations of the structure, which propagate from both walls, interfere.

Whereas the chain can orient freely inside a thick film, parallelly aligned and flattened configurations are present at the wall for all film thicknesses. Therefore, the long axes of the ellipsoid gradually turn parallel to the wall and the chain

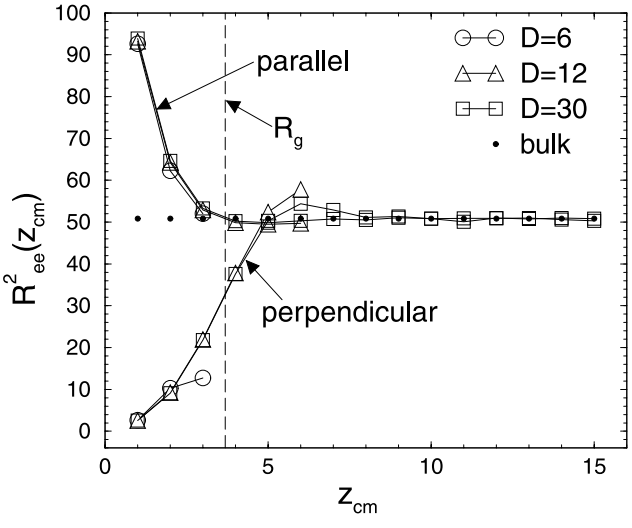

Fig. 1. Profile of the end-to-end distance, $R^2_{ee}(z_{cm})$, measured parallel and perpendicular to the wall. z_{cm} denotes the distance of the chain's center of mass from the left wall. Since the profiles are symmetric around the middle of the film, only the left half is shown. Three different thicknesses are presented: $D = 6$ ($\approx 1.5R_g$), $D = 12$, and $D = 30$ ($\approx 7.5R_g$). The bulk values of the end-to-end distance parallel to the wall, $2R^2_{ee}/3$ ($\simeq 50.82$), and of the radius of gyration, R_g (≈ 3.68), are indicated by horizontal black dots and by a vertical dashed line, respectively. All lengths are measured in units of the lattice constant.

[1] Our criterion to establish whether a configuration is equilibrated was the following: the mean-square displacements of inner monomers and the chain's center of mass were monitored parallel to the wall (Eq. (3)) until the free diffusive regime was reached. Then, we took the resulting end configuration and repeated the run. If the newly calculated mean-square displacements coincided with the initial ones for all times, the system was considered to be equilibrated.

is distorted when z_{cm} approaches the wall. The extent of these structural changes depends on film thickness. Generally, this leads to an increase in the parallel component and to a decrease in the perpendicular component of $R^2_{ee}(z_{cm})$, which is, sometimes, preceded by a slight maximum. We find such a maximum at $z_{cm} = 6$ for $D \geq 12$. It corresponds to chains which are on average preferentially oriented perpendicular to the wall. Such chains can (presumably) already touch the wall with some of their monomers and thus contribute to the large monomer density there. This interpretation is corroborated by simulations of liquid *n*-tridecane, in which the variation of the monomer distribution around the center of mass shows exactly this behavior as z_{cm} approaches the wall [64]. In our study, for $D = 12$, the chains at $z_{cm} = 6$ can reach both walls, which enhances the perpendicular component $R^2_{ee,\perp}(z_{cm} = 6)$ relative to other film thicknesses.

For the smallest thickness, $D = 6$, the film is so thin that the interference of both walls leads to a very high concentration of chains in the center at $z_{cm} = 3$, whereas their concentration is comparable to that obtained for larger D if $z_{cm} = 1$ or $z_{cm} = 2$ [22,65]. Since the layer at $z_{cm} = 3$ accomodates many chains, the ellipsoids are less prolate and their parallel orientation is more pronounced than at larger film thicknesses. This is reflected by the small value of $R^2_{ee,\perp}$ ($z_{cm} = 3$) in Fig. 1.

3.2. Example for properties averaged over the whole film: Rouse modes

In a dense melt, long range excluded volume and hydrodynamic forces are screened. Therefore, the Rouse model should provide a reliable approximation to polymer dynamics if entanglements are unimportant [39–41]. This is the case in the present simulation (remember $N = 10 < N_e \approx 37$ [47,48]). The basic variables of the (discrete) Rouse model, the Rouse modes, are given by [66]

$$\mathbf{X}_p(t) = \frac{1}{N}\sum_{n=1}^{N} \mathbf{R}_n(t)\cos\frac{(n-1/2)p\pi}{N} \quad (p = 0, 1, \ldots, N-1), \tag{1}$$

where $\mathbf{R}_n(t)$ is the position of the nth monomer at time t. The model suggests that different modes are orthogonal at all times, i.e. $\langle \mathbf{X}_p(t)\cdot\mathbf{X}_q(0)\rangle \propto \delta_{pq}$. At $t = 0$, the (static) correlation of the modes reflects structural properties of the polymers. For the bond-fluctuation model in the bulk, it turned out that the orthogonality of the modes is well satisfied if $N < N_e$ and that a very good approximation to the simulation data is obtained if local stiffness effects are taken into account via the average cosine of the bond angle θ

$$\frac{8N(N-1)}{R^2_{ee}}\langle \mathbf{X}^2_p(0)\rangle \simeq \left[\frac{1}{\sin(p\pi/2N)}\right]^2 - \frac{4(-\alpha)}{1-2(-\alpha)\cos(p\pi/N)+(-\alpha)^2}, \tag{2}$$

where $\alpha = \langle\cos\theta\rangle$ and R^2_{ee} is the mean-square end-to-end distance. The first term on the right-hand side represents the (exact) result for completely flexible, random walk chains [66] and the second is an approximate correction to it due to local stiffness [48].

Motivated by these bulk results, we determined the static Rouse mode correlation functions parallel, $\langle \mathbf{X}^{\parallel}_p(0)\cdot\mathbf{X}^{\parallel}_q(0)\rangle$, and perpendicular, $\langle \mathbf{X}^{\perp}_p(0)\cdot\mathbf{X}^{\perp}_q(0)\rangle$, to the wall for $p, q = 1, \ldots, 9$ ($= N - 1$). Representative results are shown in Figs. 2 and 3. Fig. 2 tests the orthogonality of the first Rouse mode for the smallest and largest film thicknesses studied, i.e. for $D = 6$ ($\approx 1.5R_g$) and $D = 60$ ($\approx 15R_g$). Two observations can be made: first, the self-correlation of the first mode is 1–2 orders of magnitude larger than cross-correlations with $q > 1$. Nonetheless, the cross-correlations exhibit a systematic trend. They are larger for $q = 3, 5, 7$ than for even modes and particularly pronounced for these q-values in the thinnest film. Second, the auto-correlations of $\langle[\mathbf{X}^{\parallel}_1(0)]^2\rangle$ and $2\langle[\mathbf{X}^{\perp}_1(0)]^2\rangle$ almost coincide for $D = 60$, whereas $\langle[\mathbf{X}^{\parallel}_1(0)]^2\rangle$ is about a factor of 7 larger than $2\langle[\mathbf{X}^{\perp}_1(0)]^2\rangle$ for $D = 6$. The factor 2 for the perpendicular component takes into account that $\langle[\mathbf{X}^{\parallel}_p(0)]^2\rangle$ is an average over two directions (x and y), whereas $\langle[\mathbf{X}^{\perp}_p(0)]^2\rangle$ is the correlation along one direction only.

This difference is illustrated again in Fig. 3 which shows the p-dependence of $\langle[\mathbf{X}^{\parallel}_p(0)]^2\rangle$ and $2\langle[\mathbf{X}^{\perp}_p(0)]^2\rangle$ for both film thicknesses. Whereas the parallel and perpendicular components almost coincide for $D = 60$, indicating that

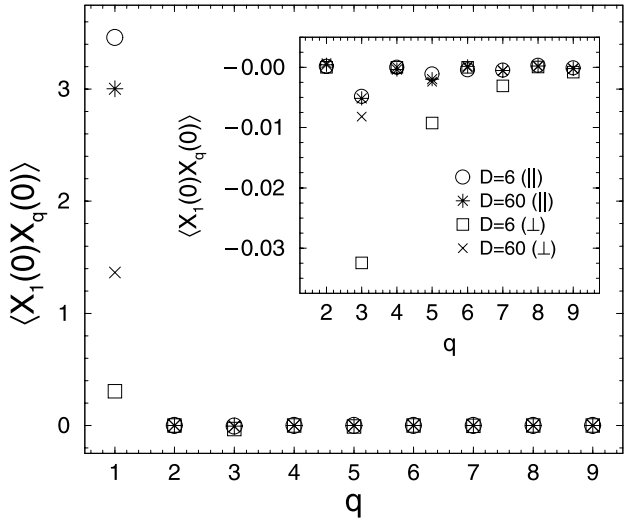

Fig. 2. Test of the orthogonality of the Rouse modes at $t = 0$. The main figure shows the parallel, $\langle \mathbf{X}^{\parallel}_1(0)\cdot\mathbf{X}^{\parallel}_q(0)\rangle$, and perpendicular components, $\langle \mathbf{X}^{\perp}_1(0)\cdot\mathbf{X}^{\perp}_q(0)\rangle$ ($q = 1, \ldots, N-1 = 9$), of the Rouse mode correlation function for $D = 6$ ($\approx 1.5R_g$) and $D = 60$ ($\approx 15R_g$; R_g (≈ 3.68) is the bulk radius of gyration). Note that the perpendicular component must be multiplied by 2 to put it on the same scale as the parallel component because $\langle \mathbf{X}^{\parallel}_1(0)\cdot X^{\parallel}_q(0)\rangle$ is the sum of the (x,y)-directions of the correlation function. The inset magnifies the results for $q = 2, \ldots, 9$. Although cross-correlations are about 1–2 orders of magnitude smaller than $\langle \mathbf{X}^{\parallel,\perp}_1(0)\cdot\mathbf{X}^{\parallel,\perp}_1(0)\rangle$, the correlation between the first mode and $q = 3, 5, 7$ is much more pronounced for the perpendicular component of the thinnest film than for larger film thicknesses.

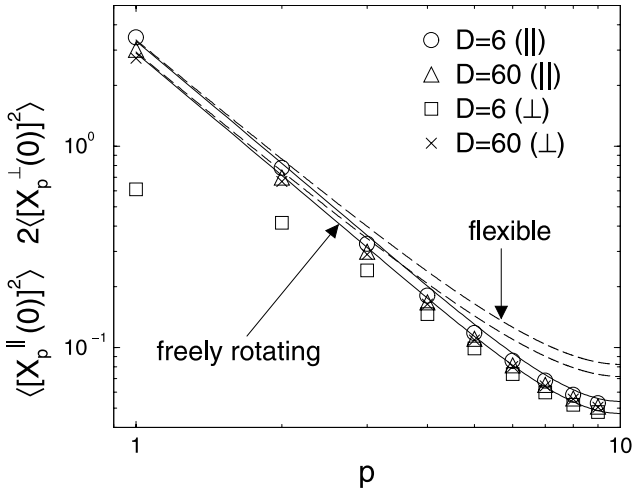

Fig. 3. Static auto-correlation of the Rouse modes parallel, $\langle [\mathbf{X}_p^{\parallel}(0)]^2 \rangle$, and perpendicular, $2\langle [\mathbf{X}_p^{\perp}(0)]^2 \rangle$, to the wall versus mode index p. The factor '2' for the perpendicular component takes into account that $\langle [\mathbf{X}_p^{\parallel}(0)]^2 \rangle$ is an average over the (x,y)-directions parallel to the wall, whereas $\langle [\mathbf{X}_p^{\perp}(0)]^2 \rangle$ is calculated along the z-direction only. Two different film thicknesses are compared: $D = 6$ ($\approx 1.5R_g$) and $D = 60$ ($\approx 15R_g$; R_g (≈ 3.68) is the bulk radius of gyration). The dashed and solid lines show $\langle [\mathbf{X}_p^{\parallel}(0)]^2 \rangle$ predicted by the Rouse model for fully flexible chains (first term on the right-hand side of Eq. (2)) and for freely rotating chains (both terms on the right-hand side of Eq. (2)), respectively. In Eq. (2), the following averages over the whole film were used for the parallel end-to-end distance, $R^2_{ee,\parallel}(D) : R^2_{ee,\parallel}(D = 6) = 59.31$, $R^2_{ee,\parallel}(D = 60) = 51.73$ (bulk value: $2R^2_{ee}/3 \simeq 50.82$). For the cosine of the bond angle, $\alpha = \langle \cos\theta \rangle$, the bulk value was inserted, i.e. $\alpha = -0.1055$.

the confinement is only a weak constraint for the average properties of the film, they deviate for small p, but converge towards one another with increasing p if $D = 6$. Qualitatively, this behavior of the thinnest film is plausible. The strong confinement makes the chains orient parallel to the wall and expand in this direction. It particularly affects the global extension of the chain, but not so much the local scales: for $D = 6$, the ratio of the end-to-end distance parallel and perpendicular to the wall is $R^2_{ee,\parallel}/R^2_{ee,\perp} \simeq 10.8$ ($R^2_{ee,\parallel} \simeq 59.31$, $R^2_{ee,\perp} \simeq 5.49$), whereas it is only $b^2_{\parallel}/b^2_{\perp} \simeq 2.9$ ($b^2_{\parallel} \simeq 4.99$, $b^2_{\perp} \simeq 1.75$) for the bond length. Since the first Rouse mode measures the overall extension of the chain, while the higher modes probe more and more the local scales along the backbone of the chain, the influence of confinement is expected to be most pronounced for $\langle [\mathbf{X}_1^{\perp}(0)]^2 \rangle$ in the thinnest film and to decrease with increasing mode index. This behavior is observed in Fig. 3. Furthermore, the figure shows that Eq. (2) also provides a good approximation to the simulation data of $\langle [\mathbf{X}_p^{\parallel}(0)]^2 \rangle$ in confined geometry if $R^2_{ee,\parallel}$ is inserted for the respective film thickness.

4. Dynamic properties of the polymer films

This section deals with the dynamic properties of the simulated polymer films. For the analysis, we consider two kinds of quantities: Translational motion is studied by various mean-square displacements, whereas reorientational relaxation is probed on the length scale of both the bond and the chain by time-displaced correlation functions. Both quantities are analyzed parallel and perpendicular to the wall and compared to predictions of the Rouse model.

4.1. A mean-square displacements

For a polymer chain in a film geometry, different mean-square displacements can be defined. Common choices are

$$g_1^{\parallel,\perp}(t) = \frac{1}{2} \sum_{n=\mathrm{iM}} \langle [\mathbf{R}_n^{\parallel,\perp}(t) - \mathbf{R}_n^{\parallel,\perp}(0)]^2 \rangle,$$

$$g_2^{\parallel,\perp}(t) = \frac{1}{2} \sum_{n=\mathrm{iM}} \langle [\mathbf{R}_n^{\parallel,\perp}(t) - \mathbf{R}_{\mathrm{cm}}^{\parallel,\perp}(t) - \mathbf{R}_n^{\parallel,\perp}(0) + \mathbf{R}_{\mathrm{cm}}^{\parallel,\perp}(0)]^2 \rangle, \tag{3}$$

$$g_3^{\parallel,\perp}(t) = \langle [\mathbf{R}_{\mathrm{cm}}^{\parallel,\perp}(t) - \mathbf{R}_{\mathrm{cm}}^{\parallel,\perp}(0)]^2 \rangle,$$

where 'iM' denotes the two inner monomers of a chain (i.e. 5 and 6), and $\mathbf{R}_n^{\parallel}(t) = (R_{x,n}(t) R_{y,n}(t))$, $\mathbf{R}_n^{\perp}(t) = R_{z,n}(t)$ and $\mathbf{R}_{\mathrm{cm}}^{\parallel}(t) = (R_{x,\mathrm{cm}}(t), R_{y,\mathrm{cm}}(t))$, $\mathbf{R}_{\mathrm{cm}}^{\perp}(t) = R_{z,\mathrm{cm}}(t)$ are the parallel and perpendicular components of the position vectors to the nth monomer and to the chain's center of mass at time t. In Eq. (3), $g_1^{\parallel,\perp}$ denotes the mean-square displacement of the two inner monomers parallel and perpendicular to the wall, $g_2^{\parallel,\perp}$ is the same displacement relative to the motion of the center of mass of the chain, and, finally, $g_3^{\parallel,\perp}$ represents the mean-square displacement of the chain's center of mass parallel and perpendicular to the wall.

In the bulk, one would expect the following behavior: at early times, the center of mass hardly moves with respect to the monomers. Therefore, $g_1(t)$ and $g_2(t)$ virtually start at the same value which is larger than that of $g_3(t)$ by about a factor of $1/N$. On the other hand, if the center of mass has displaced over the size of the chain, i.e. $g_3(t) \gtrsim R^2_{ee}$, it diffuses freely. Chain connectivity then requires that the monomers follow the motion of the center of mass. At these late times, one thus expects that $g_1(t) \propto g_3(t) = 6D_{\mathrm{cm}}t$ (D_{cm} = diffusion coefficient of the chain), and that $g_2(t)$ takes a constant value (i.e. the monomers do not move in the center-of-mass system). Due to the definition of $g_2(t)$, this constant should be proportional to R^2_g.

Fig. 4 shows that these qualitative aspects are borne out by the simulation data for the parallel displacements and are almost independent of film thickness (see panel (a)). The figure compares two extreme situations: the thinnest film thickness $D = 6$ ($\simeq 1.5R_g$), where the chains are strongly confined and oriented parallel to the walls, and the unconstrained bulk. Only at early times, there is a noticeable difference, the displacements of the film being larger than those of the bulk. These early times correpond to very local motions on the length scales of a lattice constant (=1) and of a bond. On these local scales, the differences in the local

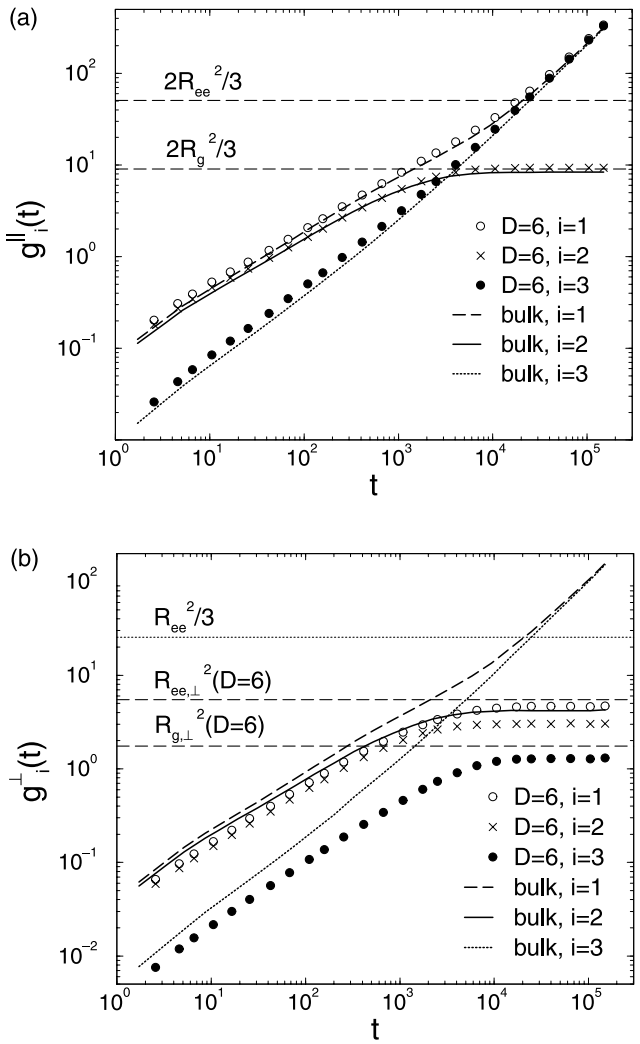

Fig. 4. Log–log plot of the time dependence of various mean-square displacements (msds) measured (a) parallel and (b) perpendicular to the wall: g_1 is the msd of the inner monomers of a chain, g_2 that of the inner monomers relative to the center of mass, and g_3 that of the chain's center of mass (Eq. (3)). The figure compares the behavior of the thinnest film ($D = 6 \approx 1.5R_g$; R_g ($\simeq$3.68) is the bulk radius of gyration) with that of the bulk. The bulk displacements were multiplied by 2/3 in panel (a) and by 1/3 in panel (b) to account for the fact that the msds of the film represent averages over two directions for the parallel component and over one direction for the perpendicular one only. In panel (a), horizontal dashed lines indicate 2/3 of the bulk end-to-end distance and the bulk radius of gyration, i.e. $2R_{ee}^2/3$ ($\simeq$50.82) and $2R_g^2/3$ ($\simeq$9.03). In panel (b), the horizontal dashed lines show the components of the end-to-end distance and of the radius of gyration perpendicular to the wall, i.e. $R_{ee,\perp}^2(D=6) \simeq 5.49$, $R_{g,\perp}^2(D=6) \simeq 1.75$, whereas the dotted horizontal line represents 1/3 of the bulk end-to-end distance $R_{ee}^2/3$ ($\simeq$25.41). Time is measured in Monte Carlo steps and the msds in units of the lattice constant.

structure between the film and the bulk must influence the dynamics.

The observed speeding up of the films could have the following explanations: on the one hand, oriented chains should have a smaller number of contacts with their neighbors compared to the bulk because they could be less intermingled. This might lead to a faster motion (see Ref. [67] for a similar argument to interpret experimental results for freely standing polymer films). On the other hand, the completely smooth walls of our model are likely to cut off the liquid structure present in the bulk. So, they remove part of the obstacles (i.e. other particles) which impede the displacement of a tagged particle. The smooth walls thus act like a 'lubricant' with respect to the bulk. This could also enhance the mobility of the nearby monomers in comparison to the bulk.

Both effects should be particularly visible for the thinnest film at early times where the motion of the monomers and chains probe the local environment around their initial positions. As time goes on, they displace over larger and larger distances and should thus average over these different environments so that their mean-square displacements resemble more and more that of bulk at the same overall density. In fact, a high precision estimate of the chain's diffusion coefficient for $D = 6$ is almost identical to (though a bit larger than) that of the bulk, i.e. $D_{cm}(D = 6)/D_{cm}^{bulk} = 1.07$.

Contrary to the parallel motion, there must be a strong impact of confinement on displacements perpendicular to the wall. Displacements in this direction are limited by the film thickness. Thus, they have to crossover to a constant proportional to D^2 at late times. At early times, one also expects the perpendicular motion of a thin film to be slower than that of the bulk due to the strongly inhomogeneous monomer and chain distributions throughout the whole film. These expectations are borne out by the simulation data (see panel (b) of Fig. 4).

4.1.1. Comparison with the Rouse model

An interesting question is to what extent the Rouse model can describe the behavior observed for the mean-square displacements. If one accepts a difference of 1–2 orders of magnitude between self- and cross-correlations as a numerical realization of $\langle \mathbf{X}_p^{\parallel,\perp}(0) \cdot \mathbf{X}_q^{\parallel,\perp}(0) \rangle \sim \delta_{pq}$, the discussion of Section 3 suggests that orthogonality of the Rouse modes, parallel and perpendicular to the wall, can be assumed, at least at $t = 0$. Extending this assumption to finite t, the mean-square displacements g_1 and g_2 can be written as follows:

$$(g_1^{\text{Rouse}})^{\parallel,\perp}(t) = g_3^{\parallel,\perp}(t) + (g_2^{\text{Rouse}})^{\parallel,\perp}(t), \tag{4}$$

$$(g_2^{\text{Rouse}})^{\parallel,\perp}(t) = 8 \sum_{p=1}^{N-1} \langle \mathbf{X}_p^{\parallel,\perp}(0)^2 \rangle \{1 - \Phi_p^{\parallel,\perp}(t)\} \cos^2\left[\frac{(n - 1/2)p\pi}{N} \right], \tag{5}$$

where

$$\Phi_p^{\parallel,\perp}(t) = \frac{\langle \mathbf{X}_p^{\parallel,\perp}(t) \cdot \mathbf{X}_p^{\parallel,\perp}(0) \rangle}{\langle \mathbf{X}_p^{\parallel,\perp}(0)^2 \rangle}. \tag{6}$$

Eqs. (4) and (5) show that the displacements g_1 and g_2 can

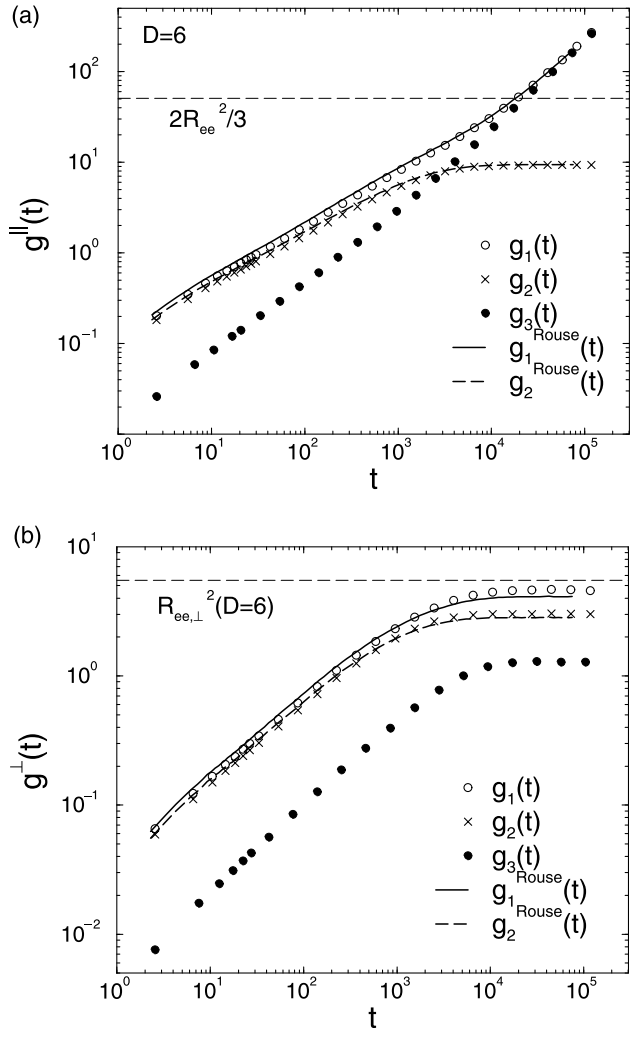

Fig. 5. Log–log plot of the time dependence of the various mean-square displacements (msds) measured (a) parallel and (b) perpendicular to the wall for $D = 6$ ($\approx 1.5R_g$; R_g (≈ 3.68) is the bulk radius of gyration): g_1 is the msd of the inner monomers of a chain, g_2 that of the inner monomers relative to the center of mass, and g_3 that of the center of mass (Eq. (3)). The figure compares the simulation data with predictions of a Rouse-like theory for g_1 and g_2 (solid line: Eq. (4); dashed line: Eq. (5)). The dashed horizontal lines in panels (a) and (b) show 2/3 of the bulk end-to-end distance ($2R_{ee}^2/3 \simeq 50.82$) and the component of the end-to-end distance perpendicular to the wall $R_{ee,\perp}^2(D = 6) \simeq 5.49$), respectively. Note that $g = 1$ corresponds to very local displacements of one lattice constant. All lengths are measured in units of the lattice constant and time in units of Monte Carlo steps.

be expressed in terms of measurable quantities, i.e. by the static and time-displaced auto-correlation functions of the Rouse modes and by the mean-square displacement of the center of mass. Their derivation is only based on the orthogonality of the Rouse modes. Thus, even if $g_3^{\|,\perp}(t), \langle \mathbf{X}_p^{\|,\perp}(0)^2 \rangle$ and $\Phi_p^{\|,\perp}(t)$ do not satisfy the predictions of the Rouse model (which is the case, even in the bulk [48], for the present model; see Section 3 and Ref. [22]), one can determine the input quantities of the right-hand side of Eqs. (4) and (5) separately in the simulation and compare the result to the simulated results for the respective displacements. Such a comparison should reveal to what extent orthogonality is preserved when correlating Rouse modes at $t = 0$ with those at $t > 0$.

Fig. 5 shows a test of this idea for both parallel (panel (a)) and perpendicular displacements (panel (b)) of the thinnest film, for which static cross-correlations between the Rouse modes were most pronounced (Fig. 2). Although the coincidence of $g_1^{\|}(t)$ and $(g_1^{\text{Rouse}})^{\|}(t)$ at late times is imposed by construction — note that $g_1^{\|}(t) \sim g_3^{\|}(t)$ as well as $(g_1^{\text{Rouse}})^{\|}(t) \sim g_3^{\|}(t)$ if $t \to \infty$, since $\Phi_p^{\|}(t \to \infty) = 0$ — the assumption of orthogonality represents a good approximation, also for the perpendicular displacements, at all times. The violation of orthogonality is more noticeable for the perpendicular component than for the parallel one. This could have been anticipated from the behavior of the static correlations (Fig. 2).

4.2. Orientational correlation functions

The relaxation of orientational correlations on different length scales along the backbone of the chain can be monitored by

$$\Phi_A(t) = \frac{\langle \mathbf{A}(t)\cdot\mathbf{A}(0)\rangle - \langle \mathbf{A}(t)\rangle\cdot\langle \mathbf{A}(0)\rangle}{\langle \mathbf{A}(0)^2\rangle - \langle \mathbf{A}(0)\rangle^2}. \tag{7}$$

For the present analysis, we chose the bond and the end-to-end vectors, i.e. $\mathbf{A}(t) = \mathbf{b}_{n,\|,\perp}$ and $\mathbf{A}(t) = \mathbf{R}_{\text{ee},\|,\perp}(t)$ ($\mathbf{b}_n$ = bond vector from monomer n to monomer $n + 1$). The corresponding correlation functions are shown in Fig. 6 for $D = 6$ where they are compared with bulk and predictions of the Rouse model, i.e.

$$\Phi_{\text{ee},\|;\perp}^{\text{Rouse}}(t) = \frac{\sum_{p\ \text{odd}} \langle \mathbf{X}_p^{\|,\perp}(t)\cdot\mathbf{X}_p^{\|,\perp}(0)\rangle \cos^2[p\pi/2N]}{\sum_{p\ \text{odd}} \langle [\mathbf{X}_p^{\|,\perp}(0)]^2\rangle \cos^2[p\pi/2N]} \tag{8}$$

$(p = 1, \ldots, N-1)$,

$$\Phi_{b,\|;\perp}^{\text{Rouse}}(t) = \frac{\sum_{n=1}^{N-1}\sum_{p=1}^{N-1} \langle \mathbf{X}_p^{\|,\perp}(t)\cdot\mathbf{X}_p^{\|,\perp}(0)\rangle \sin^2[np\pi/N]\sin^2[p\pi/2N]}{\sum_{n=1}^{N-1}\sum_{p=1}^{N-1} \langle [\mathbf{X}_p^{\|,\perp}(0)]^2\rangle \sin^2[np\pi/N]\sin^2[p\pi/2N]}. \tag{9}$$

In analogy to the discussion of the mean-square displacements, Eqs. (8) and (9) only use the assumption that the Rouse modes are orthogonal at all times. Fig. 6 allows several conclusions: the relaxation parallel to wall is much slower than the perpendicular one for both correlation functions. This difference is particularly pronounced for $D = 6$ and gradually vanishes with increasing film thicknesses (not shown here). If $D \approx 30$ ($\approx 7.5R_g$), parallel and perpendicular correlation functions (almost) coincide with one

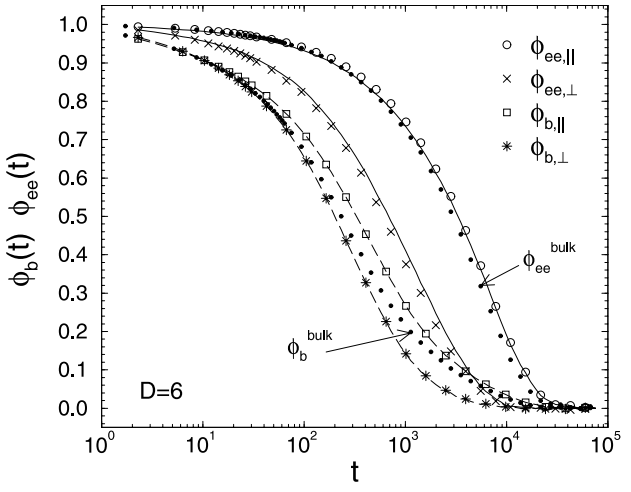

Fig. 6. Correlation functions of the end-to-end distance, $\Phi_{ee,\|}(t)$ and $\Phi_{ee,\perp}(t)$, and of the bond vector, $\Phi_{b,\|}(t)$ and $\Phi_{b,\perp}(t)$, calculated parallel ($\|$) and perpendicular ($\perp$) to the wall (Eq. (7)), versus time for the thinnest film thickness $D = 6$ ($\approx 1.5R_g$; R_g (≈ 3.68) is the bulk radius of gyration). The simulation data are represented by symbols. The solid and dashed lines show the predictions of the Rouse-like theory, Eqs. (8) and (9), for end-to-end distance and the bond vector, respectively. Note that these predictions are obtained by only assuming that the Rouse modes are orthogonal. The required input, i.e. the static and time-displaced correlation functions of the Rouse modes, are calculated independently in the simulation. Furthermore, the filled points show the correlation functions of the bulk for comparison. Time is measured in Monte Carlo steps.

another and with the bulk relaxation which is 'sandwiched' between both the components for all film thicknesses (see also Ref. [65] for a discussion of various intermediate scattering functions).

A possible explanation for the fast relaxation of $\Phi_{b,\perp}(t)$ and $\Phi_{ee,\perp}(t)$ could be as follows: imagine a polymer film with a thickness of one monomer. In this two-dimensional geometry, no relaxation perpendicular to the walls can occur. The perpendicular component of vectors, such as the bond vector or the end-to-end distance, is zero. If the film increases, the perpendicular component gradually takes a finite value, which can, however, be fairly small due to the pronounced parallel orientation of the chains (Fig. 1). Only those vectors $\mathbf{A}$ with finite perpendicular component contribute appreciably to the initial value of the correlation $\langle \mathbf{A}_\perp^2(0)\rangle$. If $\mathbf{A}_\perp(0)$ relaxes back to a more parallel orientation when time increases, the contribution $\mathbf{A}_\perp(t)\cdot\mathbf{A}_\perp(0)$ to the correlation function becomes very small and the value of $\langle \mathbf{A}_\perp(t)\cdot\mathbf{A}_\perp(0)\rangle$ should reduce considerably. Presumably, the 'fast' relaxation of the perpendicular correlation functions is thus rather a consequence of the smallness of the perpendicular component than of a rapid reorientation in this direction, since one would expect such reorientations to be suppressed by the parallel alignment of the chains for small film thicknesses.

Furthermore, Fig. 6 shows that the orthogonality of the Rouse modes is also a good assumption to model the decay of $\Phi_{b,\|}(t)$, $\Phi_{b,\perp}(t)$ and of $\Phi_{ee,\|}(t)$, $\Phi_{ee,\perp}(t)$. For the bond vector, Eq. (9) provides a perfect description, whereas Eq. (8) slightly deviates from the simulation data of the end-to-end vector relaxation. This difference between theory and simulation is presumably not a result of the strong confinement because similar deviations as observed here for the parallel component, are also present in the bulk. Therefore, they should rather be attributed to a violation of the perfect orthogonality of the Rouse modes, as it was pointed out in the discussion of Figs. 2 and 5. The difference of the accuracy to which the orthogonality assumption is valid for the bond vector and end-to-end vector decorrelations might be rationalized by the following argument: the non-orthogonal corrections of the bond and end-to-end vector correlations (i.e. nominator of Eqs. (8) and (9)) take the following form:

$$C_b^{\|,\perp}(t) = \frac{1}{N}\sum_{n=1}^{N-1}\sum_{p\neq q=1}^{N-1}\langle \mathbf{X}_p^{\|,\perp}(t)\cdot\mathbf{X}_p^{\|,\perp}(0)\rangle \sin\left(\frac{np\pi}{N}\right)\sin\left(\frac{p\pi}{2N}\right)\sin\left(\frac{nq\pi}{N}\right)\sin\left(\frac{q\pi}{2N}\right), \tag{10}$$

$$C_{ee}^{\|,\perp}(t) = 4\sum_{p\neq q=1\ (\mathrm{odd})}^{N-1}\langle \mathbf{X}_p^{\|,\perp}(t)\cdot\mathbf{X}_q^{\|,\perp}(0)\rangle\cos\left(\frac{p\pi}{2N}\right)\cos\left(\frac{q\pi}{2N}\right). \tag{11}$$

Fig. 2 suggests that the amplitude of the cross-correlations $\langle \mathbf{X}_p(t)\cdot\mathbf{X}_q(0)\rangle$ is large if both p and q are small, and that the biggest contribution should result from the modes $p = 1$ and $q = 3$. With this choice for p and q Eq. (11) shows that $\sin(p\pi/2N)\sin(q\pi/2N) \simeq 0.07$ for $N = 10$. Thus, the correction for bond vector is much smaller than the corresponding one for the end-to-end distance since $\cos(p\pi/2N)\cos(q\pi/2N) \simeq 0.88$ in this case. This might be the reason for the better coincidence of the simulation data with the Rouse model for the bond vector correlation function.

5. Summary

The purpose of this paper was to study the influence of spatial confinement on the properties of a polymer melt in an idealized situation. The simulation model consists of short (non-entangled) monodisperse chains, which are embedded between two completely smooth and impenetrable walls. Only excluded volume interactions are taken into account between the monomers and between the monomers and the walls. With this model, we investigated both static and dynamic features of polymer films of various thicknesses ranging from $D \approx 1.5R_g$ to $D \approx 15R_g$.

To interpret the static results, one has to take into account the fact that the instantaneous shape of a polymer resembles a flattened ellipsoid. Close to an impenetrable wall, the two largest principal axes of the ellipsoid align parallel to it, whereas the smallest axis orients perpendicularly [21,22]. This wall induced orientation of the chains extends over a

distance of about $2R_g$ from the wall (Fig. 1). In addition to this interfacial region, there is a bulk-like inner region with free orientation of the chains for sufficiently large film thicknesses ($D \gtrsim 5R_g$). On the other hand, as the film thickness decreases, the orientational freedom becomes more and more limited due to the interference of both walls. Therefore, the chains tend to align parallel to the walls in the inner portion of the film if $D \lesssim 4R_g$.

The spatially anisotropic geometry of the film also influences the dynamic properties of the polymer melt. Displacements perpendicular to walls are limited by the film thickness (Fig. 4) and relaxations of vectors perpendicular to the wall decay more quickly than their parallel counterparts (Fig. 6), presumably due to parallel orientation of the chains and the resulting small values for the perpendicular components of the vectors. On the other hand, the displacement parallel to the wall remains almost bulk-like and thus essentially unaffected by the confinement, even if the film thickness is of order R_g.

In the bulk, the polymer dynamics of short chains can be reasonably approximated by the Rouse theory [48]. A similar observation is made here for confined polymer melts if one uses a theory which only assumes the orthogonality of the Rouse modes, but determines their static and time-displaced correlations from the simulation (Figs. 5 and 6). These correlations deviate from the Rouse predictions (illustrated by Figs. 2 and 3, for the static correlations; see Refs. [22,48] for corresponding dynamic correlations in the film and the bulk, respectively). Chain stiffness and confinement effects have to be taken into account. Therefore, the challenge remains in understanding how these effects determine the dependence of these correlations on chain length, mode index, etc.

Acknowledgements

We are indebted to F. Eurich, T. Kreer, P. Maass, M. Müller, W. Paul and F. Varnik for helpful discussions on various aspects of this work. This study would not have been possible without a generous grant of simulation time by the HLRZ Jülich, the RHRK Kaiserslautern, the IDRIS Orsay and the computer center at the University of Mainz. Financial support by the ESF Programme on 'Experimental and Theoretical Investigation of Complex Polymer Structures' (SUPERNET) is gratefully acknowledged.

References

[1] Tirrell M, Parsonage EE. In: Thomas EL, editor. Materials science and technology, vol. 12. Weinheim: VCH, 1993. p. 653–97.
[2] Fleer GJ, Cohen Stuart MA, Scheutjens JMHM, Cosgrove T, Vincent B. Polymers at interfaces. London: Chapman & Hall, 1993.
[3] Sanchez IC, editor. Physics of polymer surfaces and interfaces. Boston: Butterworth–Heinemann, 1992.
[4] Yoon DY, Vacatello M, Smith GD. In: Binder K, editor. Monte Carlo and molecular dynamics simulations in polymer science. New York: Oxford University Press, 1995. p. 433–75.
[5] Eisenriegler E. Polymers near surfaces. Singapore: World Scientific, 1993.
[6] Eisenriegler E, Kremer K, Binder K. J Chem Phys 1982;77:6296.
[7] Bitsanis IA, Hadziioannou G. J Chem Phys 1990;92:3827.
[8] Milchev A, Binder K. Macromolecules 1996;29:343.
[9] Binder K, Milchev A, Baschnagel J. Annu Rev Mater Sci 1996;26:107.
[10] Winkler RG, Matsuda T, Yoon DY. J Chem Phys 1993;98:729.
[11] Winkler RG, Gerstmair A, Reineker P, Matsuda T, Yoon DY. Int J Quant Chem 1994;52:437.
[12] Hegger R, Grassberger P. J Phys A: Math Gen 1994;27:4069.
[13] Zajac R, Chakrabarti A. J Chem Phys 1996;104:2418.
[14] Lai P-Y. J Chem Phys 1995;103:5742.
[15] Lai P-Y. Phys Rev E 1994;49:5420.
[16] Semenov AN, Bonet-Avalos J, Johner A, Joanny J-F. Macromolecules 1996;29:2179.
[17] Semenov AN, Joanny J-F, Johner A. In: Grosberg A, editor. Theoretical and mathematical models in polymer research. San Diego: Academic Press, 1998.
[18] Johner A, Bonet-Avalos J, van der Linden CC, Semenov AN, Joanny J-F. Macromolecules 1996;29:3629.
[19] Fleer GJ, van Male J, Johner A. Macromolecules 1999;32:825.
[20] Fleer GJ, van Male J, Johner A. Macromolecules 1999;32:845.
[21] Baschnagel J, Binder K, Milchev A. In: Karim A, Kumar S, editors. Polymer surfaces, interfaces and thin films. Singapore: World Scientific, 2000. p. 1–49.
[22] Mischler C, Baschnagel J, Binder K. Polymer films in the normal-liquid and supercooled state: a review of recent Monte Carlo simulation results. Adv Colloid Interf Sci 2001 cond-mat/0012277, in press.
[23] Sen S, Cohen JM, McCoy JD, Curro JG. J Chem Phys 1994;101:9010.
[24] Phan S, Kierlik E, Rosinberg ML, Yethiraj A, Dickman R. J Chem Phys 1995;102:2141.
[25] Yethiraj A, Kumar S, Hariharan A, Schweizer KS. J Chem Phys 1994;100:4691.
[26] Brazhnik PK, Freed K, Tang H. J Chem Phys 1994;101:9143.
[27] Hooper JB, McCoy JD, Curro JG. J Chem Phys 2000;112:3090.
[28] Hooper JB, Pileggi MT, McCoy JD, Curro JG, Weinhold JD. J Chem Phys 2000;112:3094.
[29] Müller M, MacDonald LG. Macromolecules 2000;33:3902.
[30] Yethiraj A. J Chem Phys 1998;109:3269.
[31] Baschnagel J, Binder K. J Phys I, Fr 1996;6:1271.
[32] Jang JH, Mattice WL. Macromolecules 2000;33:1467.
[33] Rapold RF, Mattice WL. Macromolecules 1996;29:2457.
[34] Doruker P, Mattice WL. Macromolecules 1997;30:5520.
[35] Baschnagel J, Binder K, Doruker P, Gusev AA, Hahn O, Kremer K, Mattice WL, Müller-Plathe F, Murat M, Paul W, Santos S, Suter UW, Tries V. Adv Polym Sci 2000;152:41.
[36] Doruker P, Mattice WL. Macromolecules 1999;32:194.
[37] Vao-soongnern V, Mattice WL. Langmuir 2000;16:6757.
[38] Jang JH, Mattice WL. Polymer 1999;40:4685.
[39] Doi M, Edwards SF. Theory of polymer dynamics. Oxford: Clarendon Press, 1986.
[40] Dünweg B, Stevens M, Kremer K. In: Binder K, editor. Monte Carlo and molecular dynamics simulations in polymer science. New York: Oxford University Press, 1995. p. 125–93.
[41] Binder K, Paul W. J Polym Sci B 1997;35:1.
[42] Baschnagel J, Binder K. Macromolecules 1995;28:6808.
[43] Carmesin I, Kremer K. Macromolecules 1988;21:2819.
[44] Deutsch H-P, Binder K. J Chem Phys 1991;94:2294.
[45] Wittmann H-P, Kremer K. Comp Phys Commun 1990;61:309.
[46] Wittmann H-P, Kremer K. Comp Phys Commun 1992;71:343.
[47] Müller M, Wittmer J, Barrat J-L. Europhys Lett 2000;52:406.
[48] Kreer T, Baschnagel J, Müller M, Binder K. Macromolecules 2001;34:1105.
[49] Paul W, Binder K, Heermann DW, Kremer K. J Phys 1991;2(1):37.

[50] Paul W, Binder K, Heermann DW, Kremer K. J Chem Phys 1991;95:7726.
[51] Sokal AD. In: Binder K, editor. Monte Carlo and molecular dynamics simulations in polymer science. New York: Oxford University Press, 1995. p. 47–124.
[52] Kremer K, Binder K. Comp Phys Rep 1988;7:259.
[53] Wolfgardt M, Baschnagel J, Binder K. J Phys 2, Fr 1995;5:1035.
[54] Baschnagel J, Binder K. Macromol Theory Simul 1996;5:417.
[55] Kraus J, Müller-Buschbaum P, Kuhlmann T, Schubert DW, Stamm M. Europhys Lett 2000;49:210.
[56] Jones RL, Kumar SK, Ho DL, Briber RM, Russell TP. Nature 1999;400:147.
[57] Aronovitz JA, Nelson DR. J Physique 1986;47:1445.
[58] Šolc K, Stockmayer WH. J Chem Phys 1971;54:2756.
[59] Šolc K. J Chem Phys 1971;55:335.
[60] Cannon JW, Aronovitz JA, Goldbart P. J Phys 1991;1(1):629.
[61] Janszen HWHM, Tervoort TA, Cifra P. Macromolecules 1996;29:5678.
[62] Eurich F, Maass P. J. Chem Phys 2001;114:7655.
[63] Wang W-S, Binder K. J Phys I, Fr 1991;1:1583.
[64] Vacatello M, Yoon DY, Laskowski BC. J Chem Phys 1990;93:779.
[65] Baschnagel J, Mischler C, Binder K. J Phys IV, Fr 2000;10:7–9.
[66] Verdier PH. J Chem Phys 1966;45:2118.
[67] Ngai KL, Rizos AK, Plazek DJ. J Non-Cryst Solids 1998;235–237:435.